

Nanoparticle-Controlled Aggregation of Colloidal Tetrapods

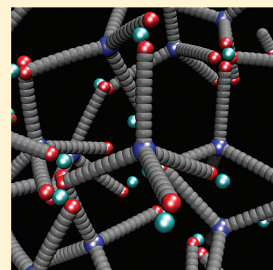
Daniel W. Sinkovits^{†,‡} and Erik Luijten^{*,‡,§}

[†]Department of Physics, University of Illinois at Urbana–Champaign, Urbana, Illinois 61801, United States

[‡]Department of Materials Science and Engineering and [§]Department of Engineering Sciences and Applied Mathematics, Northwestern University, Evanston, Illinois 60208, United States

ABSTRACT: Tetrapods are among the most promising building blocks for nanoscale self-assembly, offering various desirable features. Whereas these particles can be fabricated with remarkable precision, comparatively less is known about their aggregation behavior. Employing a novel, powerful simulation method, we demonstrate that charged nanoparticles offer considerable control over the assembly of tip-functionalized tetrapods. Extending these findings to tetrapods confined to a gas/liquid interface, we show that regular structures can be achieved even without functionalization.

KEYWORDS: Self-assembly, Monte Carlo, cluster algorithm, nanorods



The ability to synthesize monodisperse particles with a variety of well-defined shapes has spurred widespread interest in the exploration of how these particles can be used to create self-assembled structures.^{1–3} Building blocks with tetrahedral geometry, which are of great importance in molecular assembly, enjoy particular attention. CdSe,⁴ ZnO,⁵ and CdTe⁶ tetrapods have been synthesized with remarkable control over their dimensions.^{7–11} Moreover, functionalization has been demonstrated, either of the entire surface¹² or of the tips only.^{13,14} This combination of geometry, size control, and functionality has led to the consideration of tetrapods as electronic components^{15,16} and lasers.^{17–19}

Here, we consider two scenarios for the controlled self-assembly of tetrapodal building blocks. In a one-component suspension of tetrapods, we exploit functionalization to influence their pairwise interactions and demonstrate how the structure of aggregates can be controlled through manipulation of surface charge. Then, as an alternative to the creation of particles with ever-increasing complexity, we pursue modification of the effective interaction between tetrapods through addition of a second component in the form of charged nanoparticles. Binary phase diagrams offer a far richer design space than those of one-component systems, and entropic effects, particularly in size-asymmetric mixtures, can yield a wealth of aggregation phenomena, ranging from depletion attraction²⁰ to oscillatory potentials.²¹

We aim to study these scenarios by computational means. However, systems containing a mixture of large anisotropic particles and small particles pose several challenges to current theoretical and computational approaches. Density-functional theory approaches have been developed to deal with binary hard-sphere mixtures,^{22,23} but this technique is difficult to apply when the large particles are anisotropic²⁴ or when temperature-dependent interactions are involved.²² On the other hand, particle-based methods, such as molecular dynamics and Monte Carlo simulations, offer the advantage that all degrees of freedom, and hence fluctuation phenomena, are explicitly accounted for, but they are greatly hindered by the presence of a large size asymmetry.

Whereas the geometric cluster algorithm^{25–27} (GCA) resolves this issue, accelerating simulations by several orders of magnitude, it is incapable of dealing with shape anisotropy. Here, we present a powerful and highly general extension of the GCA that lifts this limitation, and apply it to the study of tetrapod–nanoparticle mixtures.

The GCA achieves its efficiency by moving entire clusters of particles. The low acceptance rate that typically accompanies collective, nonlocal displacements is avoided by exploiting geometric symmetry operations, most notably point reflections, which make it possible to design a rejection-free Monte Carlo scheme.²⁵ Although these transformations relax translational degrees of freedom, they do not relax the *orientational* degrees of freedom present in anisotropic particles, since successive point reflections can only toggle between a particle's original orientation and its inverse. Extending the geometric operations to include arbitrary plane and line reflections would eliminate this problem, allowing particles to reach all possible orientations. However, such reflections are, in general, incompatible with periodic boundary conditions. Particle positions transformed through a reflection will be subject to transformed periodic boundary conditions; if expressed using the original periodic coordinate system, distortions will arise in the interparticle distances. We observe that this limitation can be overcome by performing simulations in an isotropic space. The only isotropic three-dimensional space with finite volume is the three-dimensional surface of a hypersphere; indeed, this geometry and its two-dimensional counterpart have been employed in the past to suppress finite-size effects and to efficiently deal with long-range electrostatic interactions.^{28,29} We refer to the GCA with these two modifications, hyperspherical geometry and symmetry operations with respect to arbitrarily oriented lines and planes, as the *hyperspherical GCA* (h-GCA). Clusters are formed as in the

Received: March 23, 2011

Revised: April 26, 2011

Published: May 03, 2011

conventional GCA,²⁵ but point reflections are replaced with reflections of particles in arbitrarily oriented planes that pass through the center of the hypersphere. The new configurations that result from such cluster reflections are always accepted, that is, this remains a rejection-free Monte Carlo scheme. For testing purposes, we confirmed that results generated by this algorithm agree with conventional Metropolis Monte Carlo data for a system of asymmetric Lennard-Jones dimers. A detailed account of the methodology will appear elsewhere.³⁰ Here, we confine ourselves to introducing the concept and demonstrating that it can be used to efficiently simulate anisotropic particles in systems with large size asymmetry.

To illustrate the efficiency increase that can be achieved over the conventional Monte Carlo method, we perform simulations of rod–sphere mixtures. One hundred hard, rigid rods of length $L = 10\sigma$, each composed of 10 beads of diameter σ , are placed on the three-dimensional surface of a hypersphere with radius 8.093σ , resulting in a rod volume fraction of 5%. In addition, hard spheres of diameter σ' are present at the same volume fraction. We perform simulations for successively smaller values of σ' with resulting diameter ratios $\alpha = \sigma/\sigma'$ ranging from 1 to 9. To maintain a constant volume fraction, the number of hard spheres is increased as α^3 from 1000 to 729 000. The variation in size ratio is anticipated to lead to a rapid slowdown of the dynamic behavior.^{25,31} To quantify the efficiency of the simulations, we consider an orientational order parameter based upon the second Legendre polynomial

$$\frac{1}{N(N-1)} \sum_i \sum_{j \neq i} \left(\frac{3}{2} \left[\mathbf{s}_i \cdot \mathbf{s}_j - \frac{(\mathbf{s}_i \cdot \mathbf{r}_i)(\mathbf{s}_j \cdot \mathbf{r}_j)}{1 + \mathbf{r}_i \cdot \mathbf{r}_j} \right]^2 - \frac{1}{2} \right) \quad (1)$$

where \mathbf{r}_i is the four-dimensional unit vector on the surface of the hypersphere denoting the position of particle i and \mathbf{s}_i is the four-dimensional vector tangential to the surface of the hypersphere serving as the director of rod i ; the sums run over all rods. This is similar to the nematic order parameter,³² except that the orientations are evaluated pairwise, rather than being compared to a global director. The second term within the square brackets is a geometric correction that accounts for the fact that the directors \mathbf{s}_i and \mathbf{s}_j belong to different tangent spaces for $\mathbf{r}_i \neq \mathbf{r}_j$, due to the curvature of the hyperspherical surface. Inclusion of this term is equivalent to evaluating the dot product of the two directors after they are brought together without rotation along their common geodesic. The autocorrelation time of this parameter, expressed in CPU time, is a measure for the effort required to generate independent configurations.

Evidently, the CPU time required per configuration increases with increasing ratio α between the rod diameter and the sphere diameter, owing to the larger number of particles present. However, for simulations that employ the Metropolis Monte Carlo algorithm, where configurations evolve through local translations and rotations of the spheres and rods, the autocorrelation time increases even faster; indeed, the simulations become prohibitively slow even for moderate α (Figure 1). The behavior of the autocorrelation time in the h-GCA contrasts starkly with that in the Metropolis scheme, increasing only slowly with α . Thus, at $\alpha = 1$, the h-GCA is $\mathcal{O}(100)$ faster than a conventional algorithm; for $\alpha = 2$ this speed-up has already increased to a factor $\mathcal{O}(10^4)$. Besides the increased efficiency in crowded environments, we observe that the hyperspherical GCA also increases the efficiency of simulations of aggregating

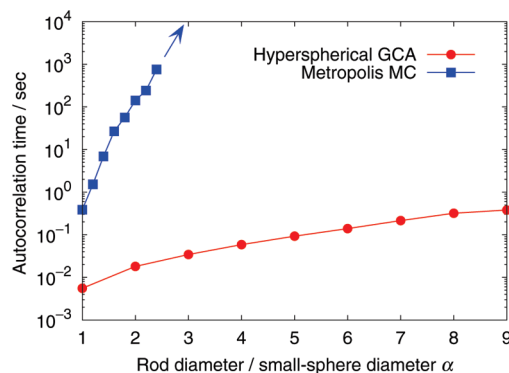


Figure 1. Comparison of the efficiency of conventional Metropolis Monte Carlo simulations and the hyperspherical GCA scheme introduced in this Letter. The autocorrelation time (obtained from simulations that have attained an equilibrium state) describes the structural relaxation of a rod–sphere mixture as a function of size asymmetry.

particles. Whereas local Monte Carlo algorithms suffer from a very low acceptance rate, the cluster-based algorithm accelerates the exploration of configuration space by permitting nonlocal moves of aggregates.³³

We apply this new simulation method to the investigation of aqueous suspensions of tetrapods. Following the typical dimensions of ZnO tetrapods,^{7,9–11} we set the arm length to $1.14 \mu\text{m}$ and the arm diameter (thickness) to 175 nm (aspect ratio 6.5). In our model, each arm is composed of 12 spherical monomers, spaced one-half diameter apart. The four arms are attached symmetrically to (and half-overlapping with) a central monomer (making for 49 monomers per tetrapod), such that each pair of arms makes an angle $\cos^{-1}(-1/3) \approx 109.47^\circ$. Under the influence of sufficiently strong, purely attractive interactions (such as van der Waals forces or depletion interactions generated by polymeric depletants), the tetrapods will aggregate irreversibly into a dense, irregular structure. Therefore, we functionalize the tips^{13,14} via a positive charge Ze at the end of each arm. To keep each tetrapod net neutral, we also place a charge $-4Ze$ at its center. The electrostatic interactions are represented by a Derjaguin–Landau–Verwey–Overbeek potential^{34,35} with a screening length of 175 nm, corresponding to a monovalent salt concentration of $3.1 \mu\text{M}$. At higher salt concentrations, we observe qualitatively similar results if the magnitude of the charges is increased to compensate for the reduced range of the interactions. The solvent is modeled implicitly as a homogeneous medium with dielectric constant 78 and temperature 298 K.

The extended structure of each tetrapod results in aggregation at remarkably low volume fractions. We investigate a system containing 60 tetrapods at a concentration of 174 pM, corresponding to a volume fraction of 0.01. The early onset of nondilute behavior can be understood by realizing that, if one replaces each tetrapod by its circumscribing sphere, these spheres would occupy a volume fraction of 0.646 (assuming the spheres do not overlap). All simulations start from a random arrangement of well-separated tetrapods. In addition to regular hyperspherical cluster moves, that is, reflections in arbitrarily oriented planes, we also introduce biased cluster moves,³¹ where the reflection plane is chosen close to the center of the first tetrapod and nearly aligned with one of its arms. Such biased moves favor small displacements. For each choice of tip valency Z we equilibrate the system for 1000 sweeps of 1000 cluster moves and

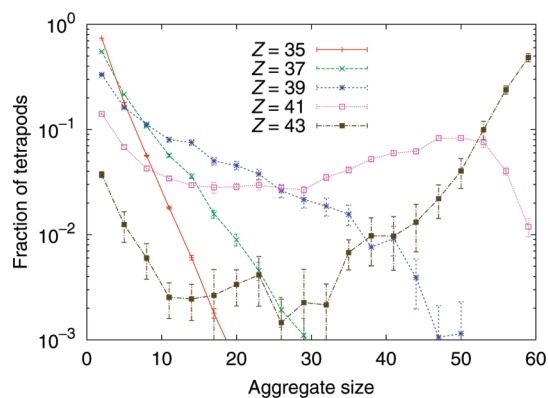


Figure 2. Fraction of tetrapods that belong to aggregates of different sizes, for different values of the tetrapod tip charge Z_e . The system contains 60 tetrapods. With increasing tip charge, the distribution shifts from a large set of isolated tetrapods, tetrapod pairs, and triplets to a small number of large aggregates. A tetrapod is considered to belong to an aggregate if its center lies within three arm diameters (arm thicknesses) from the tip of a tetrapod in the aggregate. This cutoff is based upon the first minimum in the center–tip radial distribution function.

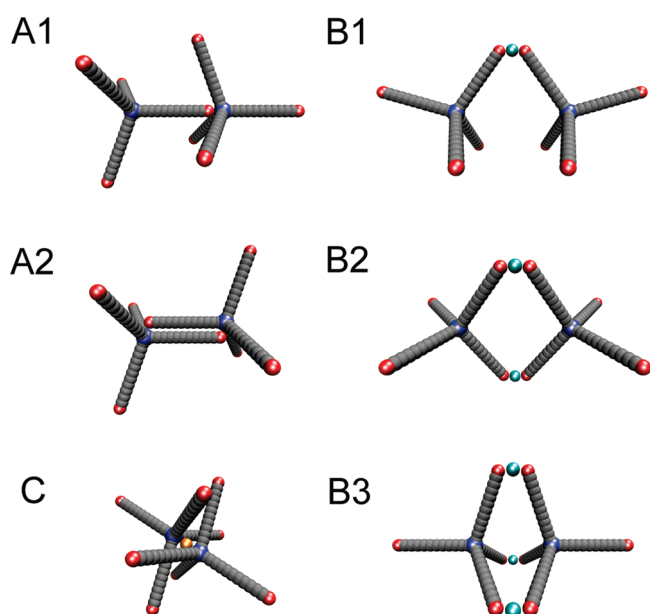


Figure 3. Classification of tetrapod pair configurations. (A1, A2) Unidirectional and bidirectional tip-to-center contacts. (B1, B2, B3) Tip-to-tip bonding induced by negatively charged nanoparticles. (C) Center-to-center bonding induced by a positive nanoparticle.

then perform 400 000 production sweeps. We find large, open aggregates with a size distribution that depends on Z (Figure 2). Within a relatively narrow range of tip charge, the system transitions from mostly unassociated tetrapods to a single aggregate and at $Z = 43$ lies within the solid–vapor coexistence region. The strong tendency to aggregate is reflected in the decorrelation time; for $Z = 37$, independent samples are separated by 100 sweeps, corresponding to approximately one independent configuration per 20 min of CPU time; for $Z = 41$ this increases to 2500 sweeps per independent sample. On average, between 24% (at $Z = 35$) and 97% (at $Z = 45$) of all

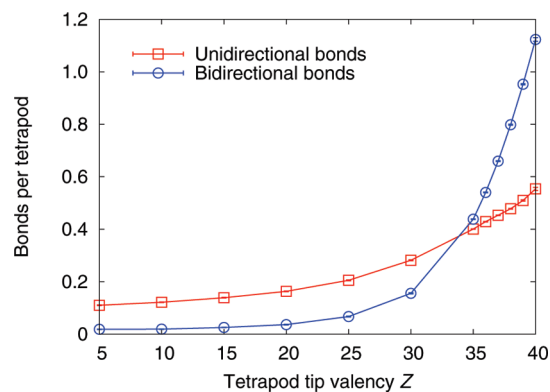


Figure 4. Number of unidirectional and bidirectional bonds per tetrapod as a function of tip charge Z_e . For $Z \leq 5$, the number of unidirectional bonds has reached a baseline value resulting from serendipitous proximity of tetrapod tips and centers. Note the rapid increase in bidirectional bonding (aligned arms, configuration A2 in Figure 3) for $Z \geq 35$.

tetrapods participate in a cluster move, and groups of bonded tetrapods break up only very rarely.

Not only the size of the aggregates depends on tip charge, but also their structure and connectivity. The charge-functionalized tetrapods can be regarded as sets of four electrical dipoles, and we observe two typical configurations for pairs of tetrapods, depicted in panels A1 and A2 of Figure 3: unidirectional bonding (A1), in which the positively charged tip of the arm of one tetrapod binds to the negatively charged center of a second tetrapod, but no tip of the latter is bound to the center of the first tetrapod, and bidirectional bonding (A2), where the arms of two tetrapods align and both tips bind to the respective center of the opposing tetrapod. At moderate tip charge, unidirectional bonding is preferred owing to the rotational freedom it provides and the consequent entropic advantage. At higher tip charge, the energetic gain of bidirectional bonding makes it dominate, although we still observe unidirectional bonding in situations where it permits bonding of tetrapods that are hindered from forming bidirectional bonds. As illustrated in Figure 4, both types of bonding increase monotonically with tip charge, but bidirectional bonding grows particularly rapidly for $Z \geq 35$. For $Z \approx 40$, the average total number of bonds per tetrapod approaches 2, corresponding to the formation of extended, chainlike aggregates.

To investigate the possibility of control over tetrapod aggregation that goes beyond variation of the tip functionality (or other means to influence the electrostatic coupling strength, namely variation of temperature or solvent polarity), we explore the role of nanoparticles in a multicomponent suspension containing tetrapods. Indeed, nanosized additives can induce a variety of effective interactions between colloids.^{20,21,36,37} In the following, we consider tetrapods of fixed tip valency $Z = +37$ and center valency $-4Z = -148$, that is, a system with significant unidirectional and bidirectional bonding (Figure 4). Nanoparticles have the same diameter as the tetrapod arms, 175 nm. We examine the effect of nanoparticles as a function of their concentration. Application of the hyperspherical GCA is essential here, as the simulations must now simultaneously relax two species with a large size asymmetry. At first, we set the nanoparticle charge q_e equal to the tetrapod center charge, $-148e$, which causes the nanoparticles to bind to the tetrapod tips. Thus, tetrapod tip-to-center bonding is suppressed, and the fraction of tips bound to a tetrapod center decreases monotonically with increasing

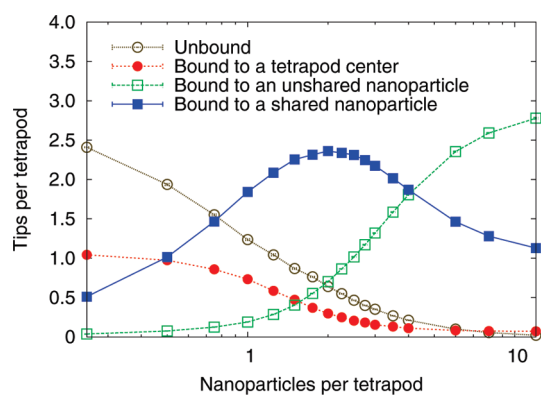


Figure 5. Dependence of tetrapod aggregation on the concentration of negatively charged nanoparticles (with tetrapod tip charge $+37e$, tetrapod center charge $-148e$, and nanoparticle charge $-148e$). Plotted are the number of tips per tetrapod that are (i) not bound to a nanoparticle or tetrapod center; (ii) bound to the center of a tetrapod; (iii) bound to a nanoparticle that is not shared with any other tip; (iv) bound to a nanoparticle shared with another tip. Here, two particles (nanoparticles and tetrapod monomers) are bound if their center-to-center distance is less than three times their diameter. Error bars are smaller than the symbol size.

nanoparticle concentration (Figure 5). However, this does not necessarily suppress aggregation, but rather alters the aggregate structure. A nanoparticle can bind to more than one tip and can create a structure of tetrapods bound via nanoparticle-mediated tip-to-tip junctions, see panels B1–B3 in Figure 3. Tip-to-tip bonding is at a maximum when there are two nanoparticles for each tetrapod (cf. curve in Figure 5 depicting the number of arms per tetrapod that are bound to a shared nanoparticle). At higher nanoparticle concentrations, tips no longer need to share a nanoparticle to achieve a low energy, and tip-to-tip bonding decreases in favor of tips bound to an unshared nanoparticle.

The observed behavior depends sensitively on the nanoparticle charge. At a concentration of two nanoparticles per tetrapod (maximal tip-to-tip bonding in Figure 5), less than one tip per tetrapod is bound to a shared nanoparticle for $|q| \leq 110$. This number doubles for $|q| = 140$ and for $|q| = 180$ more than three arms per tetrapod each participate in a junction centered around a nanoparticle. Simultaneously, the number of tips that are bound to a tetrapod center or not bound at all decreases monotonically with nanoparticle charge, similar to their dependence on nanoparticle concentration (Figure 5). However, the number of tips bound to an unshared nanoparticle remains relatively constant around 0.75 as q is varied over the range $[-80, -180]$. With increasing absolute charge, the nanoparticles start binding to previously unoccupied tips and disrupt tip-to-center bonds (thus increasing the number of tips bound to an unshared nanoparticle), but this is balanced by the increasing number of tips participating in shared junctions.

Since the number of tips belonging to such junctions is a crucial metric for the extent and structure of tetrapod aggregates, we now systematically investigate it as a function of nanoparticle charge for a range of nanoparticle concentrations. As shown in Figure 6, the behavior is qualitatively the same as curve (iv) in Figure 5 once $|q| \geq 120$, with a maximum that grows with increasing charge magnitude. Note that for the highest charge, the peak height corresponds to twice the number of nanoparticles present, consistent with a situation in which on average each nanoparticle joins two tips.

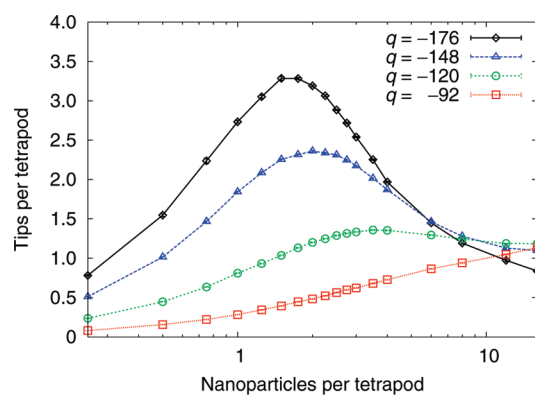


Figure 6. Characterization of nanoparticle-mediated bonding of tetrapods with center charge $-148e$. Curves represent the average number of tips per tetrapod that are bound to a *shared* negative nanoparticle as a function of nanoparticle concentration and nanoparticle valency q (i.e., the generalization of curve (iv) in Figure 5). For the highest nanoparticle charge, the peak value exceeds 3; this includes B3-type pair configurations (cf. Figure 3) and junctions where three or four tips meet one nanoparticle. (Junctions of five or more tips are rare.) Error bars are smaller than the symbol size. Calculations for intermediate values of q were performed but have been omitted here for clarity.

If positive, rather than negative, nanoparticles are added to a suspension of tetrapods, the aggregation behavior is altered in a different way. These nanoparticles migrate to the negatively charged centers of the tetrapods and again disrupt tip-to-center bonding found in the absence of nanoparticles. This displacement of tips occurs once the valency q of the nanoparticles exceeds the tip valency Z , provided that they are present in sufficiently large quantities. Indeed, at a concentration of two positive nanoparticles per tetrapod, tip-to-center bonding is decreased by 75% for $q/Z = 2$ and by more than 90% for $q/Z = 3$ (Figure 7). However, aggregation is not simply disrupted, since highly charged nanoparticles are able to act as linkers, inducing center-to-center bonding (pair configuration C in Figure 3) in which the arms of two tetrapods interlock in such a manner that their centers meet and their tips are as far apart as possible. As shown in Figure 7, this type of bonding requires a significant nanoparticle charge ($q/Z \geq 3$), as each tetrapod center carries a charge $-4Ze$, and only takes place if the nanoparticle concentration is carefully tuned. If the nanoparticles can neutralize individual tetrapod centers (i.e., if there are more than $4Z/q$ nanoparticles per tetrapod), center-to-center linking decreases abruptly, cf. Figure 7.

If the concentration of positive nanoparticles continues to be increased, a different regime is encountered, where the nanoparticles induce a depletion interaction. Since the tips of the tetrapods are also positively charged, there is a large effective excluded volume around the tips and the depletion attraction will be most pronounced there. For efficiency reasons, we reduce the interaction between nanoparticles to a hard-core repulsion, while retaining the electrostatic interactions between nanoparticles and tetrapods; this is justified by the expectation that nonadditive repulsive interactions between depletants do not strongly affect the contact strength of the depletion potential they induce.²¹ An undesirable side effect of our approximation is the unbounded accumulation of nanoparticles near tetrapod centers. However, for sufficiently weak nanoparticle charge, this leads to artifacts only at very high nanoparticle concentrations. Despite the simplification

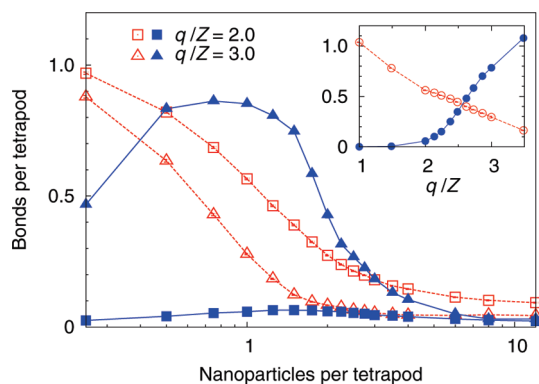


Figure 7. Positively charged nanoparticles disrupt the tip-to-center bonding of tetrapods (open symbols, dashed lines) once their valency q exceeds the tip valency Z . If the nanoparticles are present in sufficiently large quantities, they saturate the tetrapod centers (which have negative charge $-4Ze$). On the other hand, positive nanoparticles enable C-type bonding (cf. Figure 3) of tetrapods (filled symbols, solid lines), where two tetrapod centers are linked by a nanoparticle. This type of bonding becomes prominent at sufficiently high nanoparticle charge (see solid curve for $q/Z = 3$, triangular symbols), provided that the nanoparticle concentration is kept low enough to prevent neutralization of individual tetrapod centers. The inset shows how, at fixed concentration of one nanoparticle per tetrapod, C-type center-to-center bonding increases with increasing nanoparticle charge.

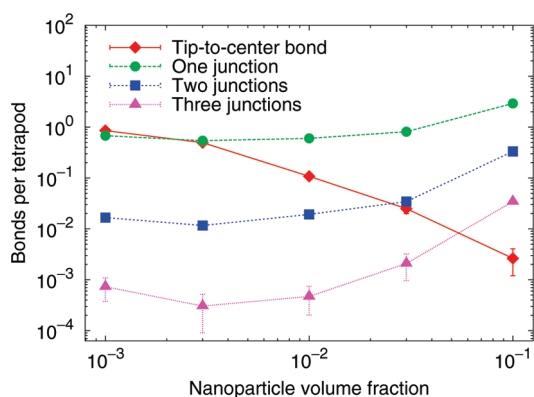


Figure 8. Aggregation of tetrapods in the presence of high concentrations of positively charged nanoparticles (tetrapod tip charge and nanoparticle charge are both $+37e$). The depletion interaction induced by the nanoparticles predominantly leads to tip-to-tip attraction. As a result, the number of tip-to-center bonds between tetrapods progressively decreases (red diamonds), and tetrapods join at their tips instead. The curves indicate the average number of bonds that each tetrapod participates in, whether it is joined to a neighboring tetrapod via a tip-to-center bond (configuration A) or via one, two, or three tip-to-tip junctions (akin to configurations B1–B3 in Figure 3, but without an intervening nanoparticle). Note the steep increase in triple-bonded tetrapods at high nanoparticle concentration, indicating the onset of large-scale structure formation.

adopted, the large size asymmetry and high number density of nanoparticles make this system prohibitively difficult to simulate for any algorithm other than the h-GCA. The system remains the same as above, consisting of 60 tetrapods and nanoparticles of fixed valency $q = +37$ (weak enough to avoid the above-mentioned artifacts). The number of nanoparticles is varied from 205 to 20 580, which corresponds to volume fractions ranging

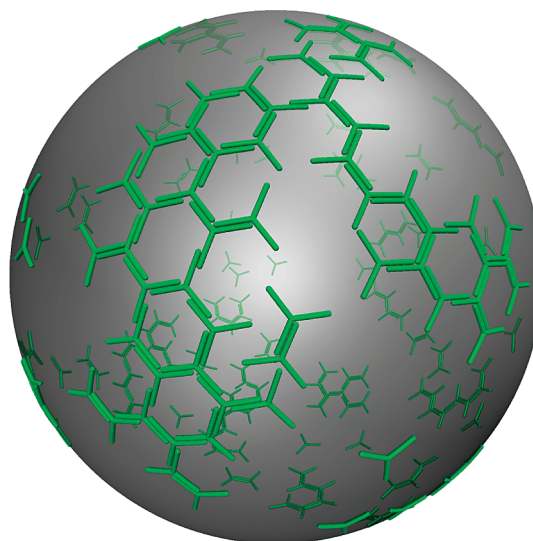


Figure 9. Snapshot of purely repulsive planar tripods aggregating on the surface of a droplet under the influence of hard-sphere depletants (modeled explicitly, but not shown for clarity).

from 10^{-3} to 10^{-1} . To quantify the effect of the nanoparticles, Figure 8 shows the average number of bonds per tetrapod, distinguishing between tip-to-center bonds (type A1 or A2, dominant in the absence of nanoparticles) and one, two, or three tip-to-tip bonds to the same neighboring tetrapod. The rapid increase, at higher nanoparticle concentrations, of triple-bonded tetrapod pairs reflects the onset of aggregate formation. Looking back, we see that tetrapods go through a remarkably rich pattern of bonding behavior upon addition of positive nanoparticles, starting from direct uni- and bidirectional tip-to-center bonding (Figure 4) to, at low concentration of positive nanoparticles, center-to-center bonding (Figure 7) to, at high nanoparticle concentration, tip-to-tip bonding (Figure 8).

In the above, we have demonstrated how electrostatically tip-functionalized tetrapods can aggregate into large-scale, open structures with a connectivity and density that can be controlled through the addition of charged nanoparticles. Both the sign of charge and the concentration of the nanoparticles play a critical role. Although the structures that we find predominantly exhibit local ordering, we believe that the work presented here provides important considerations for the design of self-assembling tetrapod structures.

Experimentally, attempts have been made to promote the formation of ordered structures by limiting the rotational freedom of tetrapods, through confinement at an air/water interface.³⁸ The resulting monolayers may find applications in, for example, photovoltaic cells owing to their charge-transport and light-adsorption properties. Frequently, three of the arms will approximately lie parallel to the interface with the fourth arm perpendicular to it. In those cases, the aggregation behavior is similar to that of planar tripods. Upon the basis of experimental realizations,^{39,40} we consider such tripods with arm length 150 nm and arm diameter 25 nm, that is, an arm aspect ratio of 6. We place 200 tripods on the surface of a spherical droplet (diameter 470 nm). Although in the simulations it is possible to assign direct attractions between tripod arms, here we opt for excluded-volume repulsions only. Subsequently, we add 5 nm nanoparticles, also with a hard-core repulsion, at a volume fraction

of 30% (corresponding to 735 000 particles). As a result, the tripods, which until then were distributed randomly, experience a strong depletion attraction. This gives rise to patches with a remarkably regular honeycomb structure (Figure 9), akin to experimentally observed structures.³⁹ We emphasize that the phenomenon demonstrated here is of purely entropic origin, with no additional attractive interactions present.

Our ability to explore tetrapod–nanoparticle mixtures hinges on the availability of a highly efficient simulation algorithm. The generalization, proposed in this Letter, of the geometric cluster algorithm²⁵ to hyperspherical geometries and the ensuing possibility of relaxing internal degrees of freedom while maintaining a rejection-free Monte Carlo scheme will have applications that go far beyond the particular system studied. One issue of potential concern would be the introduction of defects that arise in a non-Euclidean geometry. Indeed, in two-dimensional systems defined on S^2 the Poincaré–Hopf theorem implies that no defect-free nematic order can be realized. However, for the tetrapod suspensions that are the main subject of this Letter, three-dimensional systems defined on the surface of a hypersphere, this problem is absent, since S^3 is topologically equivalent to $SU(2)$ and hence is a parallelizable manifold.⁴¹ On the other hand, the intrinsic curvature of space can lead to strain, which however will decrease with increasing system size.

AUTHOR INFORMATION

Corresponding Author

*E-mail: luijten@northwestern.edu.

ACKNOWLEDGMENT

This material is based upon work supported by the National Science Foundation under Grants DMR-1006430 and DGE-0948017. We acknowledge allocation of computing time on Northwestern University's Quest cluster.

REFERENCES

- Glotzer, S. C.; Solomon, M. J. *Nat. Mater.* **2007**, *6*, 557–562.
- Jiang, S.; Chen, Q.; Tripathy, M.; Luijten, E.; Schweizer, K. S.; Granick, S. *Adv. Mater.* **2010**, *22*, 1060–1071.
- Chen, Q.; Whitmer, J. K.; Jiang, S.; Bae, S. C.; Luijten, E.; Granick, S. *Science* **2011**, *331*, 199–202.
- Manna, L.; Scher, E. C.; Alivisatos, A. P. *J. Am. Chem. Soc.* **2000**, *122*, 12700–12706.
- Dai, Y.; Zhang, Y.; Li, Q. K.; Nan, C. W. *Chem. Phys. Lett.* **2002**, *358*, 83–86.
- Manna, L.; Milliron, D. J.; Meisel, A.; Scher, E. C.; Alivisatos, A. P. *Nat. Mater.* **2003**, *2*, 382–385.
- Leung, Y. H.; Djurišić, A. B.; Gao, J.; Xie, M. H.; Chan, W. K. *Chem. Phys. Lett.* **2004**, *385*, 155–159.
- Asokan, S.; Krueger, K. M.; Colvin, V. L.; Wong, M. S. *Small* **2007**, *3*, 1164–1169.
- Zheng, K.; Xu, C. X.; Zhu, G. P.; Li, X.; Liu, J. P.; Yang, Y.; Sun, X. W. *Physica E* **2008**, *40*, 2677–2681.
- Yan, Y.; Zhou, L.; Zou, J.; Zhang, Y. *Appl. Phys. A* **2003**, *94*, 559–565.
- Newton, M. C.; Warburton, P. A. *Mater. Today* **2007**, *10*, 50–54.
- Liu, D.; Wu, W.; Qiu, Y.; Yang, S.; Xiao, S.; Wang, Q.-Q.; Ding, L.; Wang, J. *Langmuir* **2008**, *24*, 5052–5059.
- Mokari, T.; Rothenberg, E.; Popov, I.; Costi, R.; Banin, U. *Science* **2004**, *304*, 1787–1790.
- Li, F.; Yoo, W. C.; Beernink, M. B.; Stein, A. J. *Am. Chem. Soc.* **2009**, *131*, 18548–18555.
- Cui, Y.; Björk, M. T.; Liddle, J. A.; Sönnichsen, C.; Boussert, B.; Alivisatos, A. P. *Nano Lett.* **2004**, *4*, 1093–1098.
- Teich-McGoldrick, S. L.; Bellanger, M.; Caussanel, M.; Tsetseris, L.; Pantelides, S. T.; Glotzer, S. C.; Schimpf, R. D. *Nano Lett.* **2009**, *9*, 3683–3688.
- Szarko, J. M.; Song, J. K.; Blackledge, C. W.; Swart, I.; Leone, S. R.; Li, S.; Zhao, Y. *Chem. Phys. Lett.* **2005**, *404*, 171–176.
- Mondia, J. P.; Sharma, R.; Schäfer, J.; Smith, W.; Zhao, Y. P.; Lu, Z. H.; Wang, L. J. *Appl. Phys. Lett.* **2008**, *93*, 121102.
- Zalamai, V. V.; Ursaki, V. V.; Tiginyanu, I. M.; Burlacu, A.; Rusu, E. V.; Klingshirn, C.; Fallert, J.; Sartor, J.; Kalt, H. *Appl. Phys. B* **2010**, *99*, 215–222.
- Asakura, S.; Oosawa, F. *J. Chem. Phys.* **1954**, *22*, 1255–1256.
- Louis, A. A.; Roth, R. J. *Phys.: Condens. Matter* **2001**, *13*, L777–L784.
- Götzmann, B.; Roth, R.; Dietrich, S.; Dijkstra, M.; Evans, R. *Europhys. Lett.* **1999**, *47*, 398–404.
- Roth, R.; Evans, R.; Dietrich, S. *Phys. Rev. E* **2000**, *62*, 5360–5377.
- König, P.-M.; Roth, R.; Dietrich, S. *Phys. Rev. E* **2006**, *74*, 041404.
- Liu, J.; Luijten, E. *Phys. Rev. Lett.* **2004**, *92*, 035504.
- Day, C. *Phys. Today* **2004**, *57*, 25–27.
- Luijten, E. *Comput. Sci. Eng.* **2006**, *8*, 20–29.
- Hansen, J. P.; Levesque, D.; Weis, J. J. *Phys. Rev. Lett.* **1979**, *43*, 979–982.
- Caillol, J. M.; Levesque, D. *J. Chem. Phys.* **1991**, *94*, 597–607.
- Sinkovits, D. W.; Barr, S. A.; Luijten, E. manuscript in preparation.
- Liu, J.; Luijten, E. *Phys. Rev. E* **2005**, *71*, 066701.
- Collings, P. J.; Hird, M. *Introduction to Liquid Crystals: Chemistry and Physics*; Taylor & Francis: London, 1997.
- Winkler, A.; Sinkovits, D. W.; Luijten, E. manuscript in preparation.
- Derjaguin, B. V.; Landau, L. *Acta Physicochim. URSS* **1941**, *14*, 633–662.
- Verwey, E. J.; Overbeek, J. T. G. *Theory of the Stability of Lyophobic Colloids*; Elsevier: Amsterdam, 1948.
- Tohver, V.; Smay, J. E.; Braem, A.; Braun, P. V.; Lewis, J. A. *Proc. Natl. Acad. Sci. U.S.A.* **2001**, *98*, 8950–8954.
- Liu, J.; Luijten, E. *Phys. Rev. Lett.* **2004**, *93*, 247802.
- Goodman, M. D.; Zhao, L.; DeRocher, K. A.; Wang, J.; Mallapragada, S. K.; Lin, Z. *ACS Nano* **2010**, *4*, 2043–2050.
- Maksimuk, S.; Teng, X.; Yang, H. *Phys. Chem. Chem. Phys.* **2006**, *8*, 4660–4663.
- Watt, J.; Young, N.; Haigh, S.; Kirkland, A.; Tilley, R. D. *Adv. Mater.* **2009**, *21*, 2288–2293.
- Frankel, T. *The Geometry of Physics*; Cambridge University Press: Cambridge, 1997.